

A Bayesian Flow Network Framework for Chemistry Tasks

Nianze TAO, Minori ABE

Department of Chemistry,
Graduate School of Advanced Science and Engineering,
Hiroshima University, Higashi-Hiroshima, Japan
{tao-nianze,minoria}@hiroshima-u.ac.jp

July, 2024

Abstract

In this work, we introduce ChemBFN, a language model that handles chemistry tasks based on Bayesian flow networks working on discrete data. A new accuracy schedule is proposed to improve the sampling quality by significantly reducing the reconstruction loss. We show evidence that our method is appropriate for generating molecules with satisfied diversity even when a smaller number of sampling steps is used. A classifier-free guidance method is adapted for conditional generation. It is also worthwhile to point out that after generative training, our model can be fine-tuned on regression and classification tasks with the state-of-the-art performance, which opens the gate of building all-in-one models in a single module style. Our model has been open sourced at <https://github.com/Augus1999/bayesian-flow-network-for-chemistry>.

1 Introduction

Autoregressive models (ARs) including SMILES-based or fragment-based models¹⁻⁴ that leverage the power of language models (LMs) and graph-based models⁵⁻⁷ coupled with advanced techniques such as Monte Carlo tree search^{6,7} have been proved their success in several *de novo* design benchmarks^{4,8} consisted of drug-like molecules. The constraint of ARs, i.e., the number of sampling steps is the size of generated object, however, limits the potential of generating large molecules. Conversely, the recently emerging denoising-diffusion models⁹ (DMs) offer a way to generate objects of any size within a fixed sequence of sampling process. However, it has been pointed out in the research of C. Vignac *et al*¹⁰ that SMILES-based models generally worked better than graph DMs even when a dedicatedly designed discrete diffusion method was applied.

Bayesian flow networks¹¹ (BFNs) are in a different category of generative models that decouple the sampling process with the size of generated objects as well. Different from DMs, BFNs directly work on the parameters of data distributions which naturally enable them to handle both continuous (including discretised) and discrete data without any data preprocessing or change of (mathematical) framework. Although the authors of BFN showed evidence in the origin paper¹¹ that BFN advantaged over discrete DMs on discrete data generating, e.g., text generation, the recent researches considering *de novo* molecule design only successfully employed it on continuous and discretised data, e.g., 3D molecular conformation generation¹² rather than language-like representations such as SMILES¹³ or SELFIES.¹⁴ One potential reason discouraging the application to text generation is the lack of *exact* analytical expression for the accuracy schedule $\beta(t)$, one critical component of BFNs, in the discrete case, while the speculated quadratic $\beta(t)$ in the original paper is, as admitted by the authors,¹¹ suboptimal.

In this paper, we introduce ChemBFN, a Bayesian Flow Network framework for Chemistry tasks, that leverages our newly proposed accuracy schedule and transformer¹⁵ encoder model to generate 1D language-like molecular representations e.g., SMILES and SELFIES. The experiments demonstrated that models with our accuracy schedule outperform those with the quadratic accuracy schedule. Besides,

the generative training of BFN method can be a powerful pretraining strategy for downstream tasks in molecular property predictions, including regressions and classifications, and reaction yield predictions.

2 Methods

2.1 Model Architecture

Our model is an adaptation of DiT¹⁶ model. The differences in our implementation include (1) the use of categorical distributions rather than image embeddings for input tokens because we are not dealing with images; (2) logits output that are then transformed into probabilities by softmax function; (3) the replacement of activation function with SELU¹⁷ function; (4) the use of a 2-layer MLP to form the time embedding since “time” in BFN is continuous from 0 to 1; (5) the employment of XPOS¹⁸ variation of rotary positional embedding.¹⁹ The architecture is shown in Figure 1.

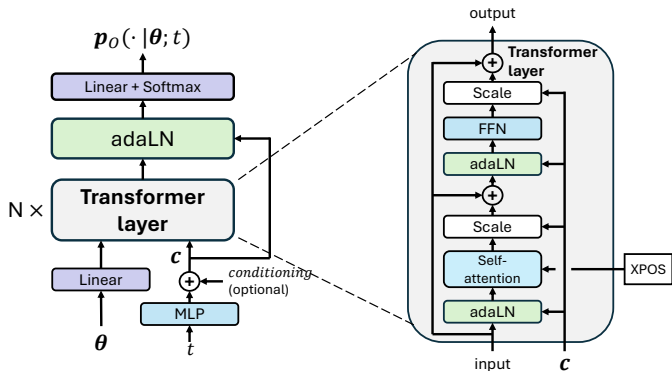


Figure 1: Visualised scheme of our model. The architecture is inspired by DiT.¹⁶ The multi-head self-attention layers did not use causal masking which is the same as BERT²⁰ while we replaced the commonly used positional embedding method (absolute positional embedding used in DiT, BERT and RoBERTa²¹ models) with the novel XPOS¹⁸ variation of rotary positional embedding.¹⁹ Note that each FFN (feed-forward network) layer adsorbs a dropout layer.

Following the notations of the BFN paper,¹¹ the parameter of categorical distributions inputted into the neural network is denoted by $\theta = (\theta^{(1)}, \theta^{(2)}, \dots, \theta^{(D)}) \in [0, 1]^{KD}$ (K is the number of categories, D is the number of input data, and $\theta^{(i)}$ is the i^{th} data) and the output distribution at time step t is denoted by $\mathbf{p}_O(\cdot | \theta; t) \in [0, 1]^{KD}$. We denote the sum of time embedding vector and conditioning vector as \mathbf{c} . A null conditioning ϕ is equivalent to a zero vector $\mathbf{0}$.

In each experiment described in the later text, we employed the same hyperparameters of the model except category number K that depends on molecular representations. The 2-layer MLP with SELU activation has the shape of [1, 256, 512]. We employed 12 Transformer layers, of which had 8 attention heads each, with the attention temperature²² $\tau = \sqrt{2d_h}$ (d_h is the feature number of each attention head). The dropout rate was 0.01 and the hidden feature number was 512. These settings lead to a total learnable parameters of the model of the magnitude of 54M.

2.2 A New Accuracy Schedule

Ideally, an accuracy schedule function $\beta(t)$ drives the expectation of entropy of the input distribution $\mathbb{E}_{\mathbf{p}_F(\theta|\mathbf{x};t)} H[\mathbf{p}_I(\mathbf{x}|\theta)]$ to decrease linearly with t , where \mathbf{x} stands for the clear *data*, $\mathbf{p}_F(\theta|\mathbf{x};t)$ represents *Bayesian flow distribution*, and $\mathbf{p}_I(\mathbf{x}|\theta)$ is the *input distribution* as denoted in the origin paper.¹¹ The mathematical difficulty of deriving the expectation analytically in the discrete case compels us to speculate from intuition. The authors of BFN claimed that “ $\beta(t) = t^2\beta(1)$ was a reasonable approximation”, but disclosed later that finding a suitable value for the hyperparameter $\beta(1)$ was not an easy job.¹¹

Here, we give our estimation of $\beta(t)$. If we estimate the expected entropy of the input distribution (denoted as E for short) as $E \sim f(K)e^{-\frac{K}{4}\beta(t)}$, then the relationship $E(t) = (1-t)E(0) + tE(1)$ that

eliminates the unknown function $f(K)$ gives us

$$\beta(t) = -\frac{4}{K} \ln \left(1 - t + te^{-\frac{K}{4}\beta(1)} \right) \quad (1)$$

and the corresponding

$$\alpha(t) = \frac{d\beta}{dt} = \frac{4}{K} \frac{1 - e^{-\frac{K}{4}\beta(1)}}{1 - t + te^{-\frac{K}{4}\beta(1)}}, \quad (2)$$

where $\beta(1)$ is still a hyperparameter. Equation (2) changes the continuous time loss L^∞ to

$$L^\infty(\mathbf{x}) = \frac{K}{2} \mathbb{E}_{t \sim U(0,1), \mathbf{p}_F(\boldsymbol{\theta}|\mathbf{x};t)} \left(\alpha(t) \| \mathbf{e}_\mathbf{x} - \mathbf{e}(\hat{\boldsymbol{\theta}}; t) \|^2 \right), \quad (3)$$

where $\mathbf{e}_\mathbf{x}$ is the one-hot representation of data \mathbf{x} while $\mathbf{e}(\hat{\boldsymbol{\theta}}; t)$ is the predicted categorical distribution of data \mathbf{x} at time t . Note that when $\beta(1)$ is large, $\alpha(1)$ goes to extremely large. Therefore, we limit $\alpha(1) \leq 32\beta(1)$, from which

$$\beta(1)_{max} \approx 20.4054/K \quad (4)$$

is obtained. An example of how our accuracy schedule looks different from original one is plotted in Figure 2. We shall show in the later experiments that our $\beta(t)$ in Equation (1) works better than quadratic ones.

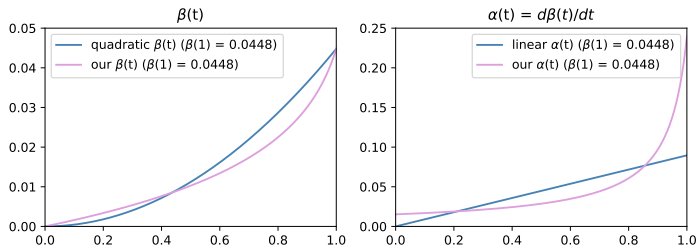


Figure 2: Comparing our accuracy schedule with quadratic accuracy schedule initialised with the same value of $\beta(1)$. (Left) Accuracy schedules $\beta(t)$. (Right) The accuracy rates $\alpha(t)$. Note that our $\beta(t)$ does not deviate too much from quadratic one, yet the rate (derivative) differs substantially as t goes to 1.

2.3 Datasets and Benchmarks

Two benchmarks – MOSES⁸ and GuacaMol⁴ – were used to evaluate the generative performance, e.g., the similarity between generated molecules and training molecules, of ChemBFN. We reported the distribution-learning metrics of these benchmarks in Section 3.

The QM9²³ dataset was employed to study the capability of conditional generation of our method. We randomly selected 110k molecules, before which 3054 invalid data were removed, with the triple $(\epsilon_{HOMO}, \epsilon_{LUMO}, \Delta\epsilon_{HOMO-LUMO})$ as the conditioning label to form the training set.

In order to evaluate the downstream performance, 40M unique SMILES and 190M unique SMILES strings were randomly selected from ZINC15²⁴ database that formed two pretraining sets. The model trained on the 40M set was finetuned on several regression (ESOL, FreeSolv, and Lipo) and classification (BBBP, BACE, ClinTox, and HIV) subsets of widely used MoleculeNet²⁵ benchmark. Each dataset was split into training/validation/testing sets in the ratio of 80/10/10 following the scaffold splitting method proposed in DeepChem²⁶ project. We reported ROC-AUC (area under receiver operating characteristic curve) for classification tasks and RMSE (root-mean squared error) for regression tasks in Section 3.

The USPTO-50k²⁷ dataset, Buchwald-Hartwig and Suzuki-Miyaura reaction yield datasets from high-throughput experiments (HTE) cleaned by P. Schwaller *et al*²⁸ were employed to train the model to predict reaction yield. We report coefficient of determination (R^2 score) on testing sets in Section 3.

AqSolDB,²⁹ a more challenging solubility dataset containing more species than ESOL, was used to investigate the effect of the size of pretraining data. A training/validation/testing (80/10/10) split was generated using scaffold splitting method. Testing MAE (mean absolute error) and RMSE were reported in Section 3.

For SMILES representation, we developed a universal tokenizer that generates a fixed number (specifically $K = 246$) of unique vocabulary for any collection of molecules. The similar strategy was not applicable to SELFIES strings, which were translated from SMILES via official *selfies*¹⁴ package, hereby the vocabulary should be computed separately for each dataset and the category number K varies. Note that we include three special tokens $\langle \text{start} \rangle$, $\langle \text{end} \rangle$, and $\langle \text{pad} \rangle$ in the vocabulary.

2.4 Fine-tuning Strategy

Similar to the strategy of ChemBERTa models,^{30,31} the embedding, denoted as $\psi'_{\langle \text{start} \rangle}$, of $\langle \text{start} \rangle$ token at time $t = 1$ was used as a fingerprint for downstream tasks. A 2-layer MLP absorbing a dropout layer is used as the prediction head. We replace the input distribution in generative mode with the one-hot representation of data (token), i.e., $\theta \leftarrow \mathbf{e}_x = (\mathbf{e}_{\langle \text{start} \rangle}, \dots, \mathbf{e}_{\langle \text{end} \rangle}) \in \{0, 1\}^{KD}$ in this stage. A visualised scheme is in Figure 3.

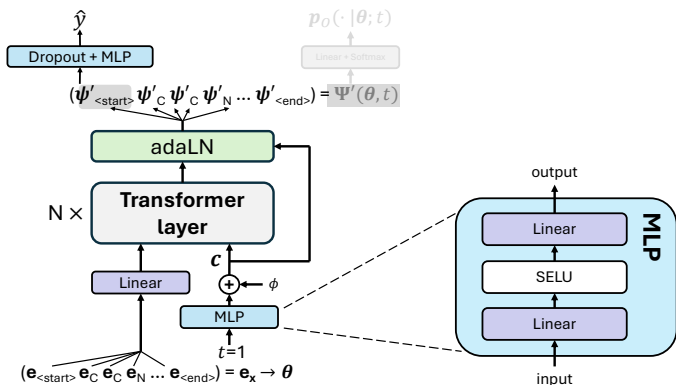


Figure 3: The fine-tuning strategy of our model. The predicted label $\hat{y} \in \mathbb{R}^n$ is mapped by a MLP from the embedding of $\langle \text{start} \rangle$ token $\psi'_{\langle \text{start} \rangle}$ restricted by $t = 1$. The MLP used here had 2 linear layers with a SELU activation function between them in a size of $[512, 256, n]$. Note that at prediction mode, the linear layer that maps latent vectors to output distributions is not activated; The conditioning is biased to null ϕ ; All $\langle \text{pad} \rangle$ tokens are masked out in attention.

3 Experiments and Results

3.1 Unconditional Generation

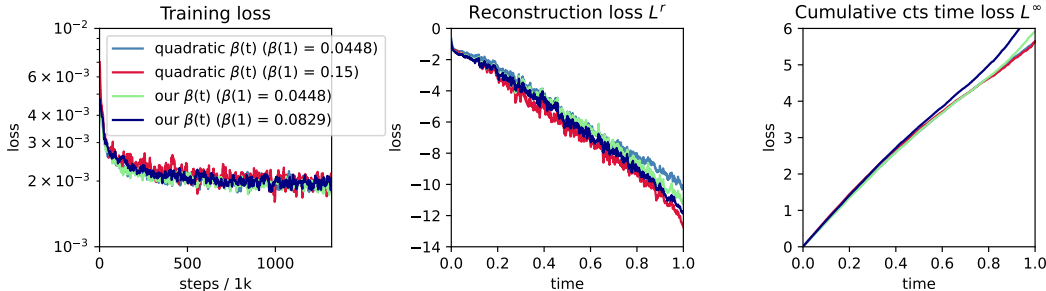


Figure 4: Visualisation of the impact on training loss, reconstruction loss L^r and cts time loss L^∞ of different accuracy schedules with different values of $\beta(1)$. L^r and L^∞ were computed on 1k discretised steps after training.

We first evaluate the effect of different $\beta(t)$ with different values of $\beta(1)$ using MOSES dataset. We reported the validity, FCD on scaffold set, SNN on scaffold set, Frag on scaffold set, Scaf on scaffold set, Filters, and Novelty scores computed by MOSES program in Table 1 together with reconstruction loss $L^r = -\mathbb{E}_{\mathbf{p}_F(\theta|\mathbf{x};t)} \ln \mathbf{p}_O(\mathbf{x}|\theta;t)$ and continuous time loss L^∞ in Figure 4. It is clear that raising

$\beta(1)$ in both quadratic and our schedules did not have obvious influence on training loss but lowered L^r , while our schedule lead to a lower loss when $\beta(1)$ was the same. The effect on L^∞ was subtle. However, after we calculated the R^2 values of the cumulative L^∞ curves, we found that while using quadratic $\beta(t)$ the curve became more distorted when $\beta(1)$ was larger ($R^2|_{\beta(1)=0.0448} = 0.995$ while $R^2|_{\beta(1)=0.15} = 0.992$); After switching to our $\beta(t)$ the curves were more linear (i.e., L^∞ was more uniform) and the linearity was not affected by the value of $\beta(1)$ ($R^2|_{\beta(1)=0.0448} = R^2|_{\beta(1)=0.0829} = 0.997$). The metrics in Table 1 provide more quantitative evidences that our $\beta(t)$ is more optimal. It is notable that a larger $\beta(1)$ value usually result to better scores. Therefore, we conclude here that our proposed $\beta(t)$ with $\beta(1) = \beta(1)_{max} = 20.4054/K$ is a more optimal solution in discrete BFNs.

Table 1: Comparing scores of MOSES benchmark when varying $\beta(1)$ value of different accuracy schedules. \uparrow indicates that the higher is better and \downarrow stands for the contrary. The best results are in **bold**. We used a sampling step of 1k.

	$\beta(1)$	Valid \uparrow	FCD \downarrow	SNN \uparrow	Frag \uparrow	Scaf \uparrow	Filters \uparrow	Novelty \uparrow
quadratic	0.15	0.893	3.438	0.559	0.985	0.095	0.982	0.900
	0.0829	0.895	3.772	0.551	0.984	0.096	0.985	0.900
	0.0448	0.899	3.902	0.561	0.988	0.089	0.986	0.887
ours	0.0829	0.900	2.731	0.563	0.990	0.091	0.987	0.886
	0.0448	0.900	3.580	0.568	0.987	0.075	0.987	0.877

In the above experiments, we used a dynamic padding strategy, i.e., each batch were padded to the maximum length of that batch, to reduce the training time. In the following experiments, global padding strategy, i.e., padding all batches to a global maximum length, was employed to compare with dynamic strategy on both MOSES and GuacaMol benchmarks. The results were summarised in Table 2. We found that the global padding method benefited the performance. In the following experiment, we therefore employed the global padding method in generative tasks.

Table 2: Scores of MOSES and GuacaMol benchmarks when different padding strategies were used during training. \uparrow for higher is better and \downarrow for contrary. The best results are in **bold**. We used a sampling step of 1k.

Strategy	MOSES						
	Valid \uparrow	FCD \downarrow	SNN \uparrow	Frag \uparrow	Scaf \uparrow	Filters \uparrow	Novelty \uparrow
dynamic	0.900	2.731	0.563	0.990	0.091	0.987	0.886
global	0.916	2.730	0.565	0.990	0.094	0.987	0.880
	GuacaMol						
	Valid \uparrow	Unique \uparrow	Novelty \uparrow	KL Divergence \uparrow	FCD \uparrow		
dynamic	0.799	0.815	0.975	0.810	0.370		
global	0.807	0.818	0.975	0.808	0.399		

Finally, we trained models applying the above optimal settings (i.e., $\beta(1) = 20.4054/K$ and global padding) on MOSES and GuacaMol datasets. Both SMILES and SELFIES versions were implemented. The comparison with published state-of-the-art (SOTA) models^{1-5,7,10} are summarised in Table 3, Table 4, and Table 5. We found that (1) except FCD, metrics of both SMILES version and SELFIES version were close to SOTA performance. (2) number of sampling step as expected affected the validity of generated molecules (for SMILES version only because SELFIES *always* gives valid molecules¹⁴), but dropping from 1k steps to 100 steps did not degrade the performance a lot. If lower validity is acceptable, only sampling 10 steps significantly reduce the computational time without much impact on other qualities. Larger FCD (in the term of GuacaMol is lower FCD score) is a hint that BFNs learn the grammar of molecules rather than the way of combining characters within the dataset.

Table 3: Testing metrics on MOSES test set compared with SOTA models. The metrics of all other models were copied from the original paper. \uparrow for the higher is better. (10, 100, 1k) are the number of sampling steps. * for SELFIES version. The best results are in **bold**.

Method		Valid \uparrow	Unique@1k \uparrow	Unique@10k \uparrow	IntDiv \uparrow	IntDiv ₂ \uparrow	Novelty \uparrow
ARs	JTN-VAE ³	1.0	1.0	1.0	0.855	0.850	0.913
	LatentGAN ¹	0.897	1.0	0.997	0.857	0.851	0.950
	GraphINVENT ⁵	0.964	1.0	0.998	0.857	0.851	–
	MolGPT ²	0.994	–	1.0	0.857	0.851	0.797
DMs	DiGress ¹⁰	0.857	–	1.0	–	–	0.950
BFNs	ChemBFN ₁₀	0.835	1.0	0.999	0.851	0.844	0.921
	ChemBFN ₁₀₀	0.911	1.0	0.998	0.837	0.831	0.884
	ChemBFN _{1k}	0.916	1.0	0.998	0.836	0.830	0.880
	ChemBFN ₁₀ *	1.0	1.0	1.0	0.860	0.855	0.991
	ChemBFN ₁₀₀ *	1.0	1.0	1.0	0.848	0.842	0.947
	ChemBFN _{1k} *	1.0	1.0	1.0	0.847	0.841	0.940

Table 4: Metrics on MOSES **scaffold** test set. Settings are the same as Table 3 while \downarrow for the lower is better.

Method		FCD \downarrow	SNN \uparrow	Frag \uparrow	Scaff \uparrow	Filters \uparrow
ARs	JTN-VAE ³	0.938	0.519	0.995	0.101	0.976
	LatentGAN ¹	0.828	0.513	0.997	0.107	0.974
	GraphINVENT ⁵	1.223	0.539	0.986	0.127	0.950
DMs	DiGress ¹⁰	1.19	0.52	–	0.148	0.971
BFNs	ChemBFN ₁₀	2.768	0.533	0.988	0.145	0.976
	ChemBFN ₁₀₀	2.604	0.562	0.991	0.103	0.985
	ChemBFN _{1k}	2.730	0.565	0.990	0.094	0.986
	ChemBFN ₁₀ *	11.79	0.422	0.965	0.118	0.806
	ChemBFN ₁₀₀ *	4.802	0.517	0.976	0.141	0.955
	ChemBFN _{1k} *	4.473	0.524	0.976	0.141	0.962

Table 5: Testing metrics on GuacaMol distribution-learning tasks. Settings are the same as Table 3.

Method		Valid \uparrow	Unique \uparrow	Novelty \uparrow	KL Divergence \uparrow	FCD \uparrow
ARs	MolGPT ²	0.981	0.998	1.0	0.992	0.907
	SMILES LSTM ⁴	0.959	1.0	0.912	0.991	0.913
	VGAE-MCTS ⁷	1.0	1.0	1.0	0.659	0.009
DMs	DiGress ¹⁰	0.852	1.0	0.999	0.929	0.680
BFNs	ChemBFN _{1k}	0.807	0.818	0.975	0.808	0.399
	ChemBFN ₁₀ *	1.0	0.853	1.0	0.451	0.000
	ChemBFN ₁₀₀ *	1.0	0.846	0.994	0.803	0.110
	ChemBFN _{1k} *	1.0	0.850	0.994	0.811	0.142

3.2 Conditional Generation of Small Molecules

The classifier-free guidance³² method is easily adapted into BFN, where only the computing of output distribution needs changing during sampling process. The pseudocode of computing discrete output distribution is presented in Algorithm 1. In the experiment, we jointly trained a model conditional and unconditional on QM9 dataset with an unconditional rate $p_{uncond} = 0.2$. In the sampling stage, w was set to 4. We sampled 10 molecules using the label $[-0.249, 0.0615, 0.3105]$ that was transformed to \mathbf{y} via a trained 2-layer MLP. 10 unconditioned samples were generated as a control group. RDKit³³ was employed to generate the 3D conformations, then the geometry optimisations and energy calculations were performed via PySCF³⁴ at B3LYP/6-31G(2df,p) level of accuracy. The results of MAE between calculated values and labels are presented in Table 6. The conditioned samples are displayed in Figure 5.

Algorithm 1 Invoking classifier-free guidance into output distribution

Require: $w \in \mathbb{R}$, conditioning vector \mathbf{y}

function DISCRETE_OUTPUT_DISTRIBUTION($\boldsymbol{\theta} \in [0, 1]^{KD}$, $t \in [0, 1]$, $\mathbf{y} \in \mathbb{R}^f$)

 Input ($\boldsymbol{\theta}$, t , \mathbf{y}) to network, receive $\Psi(\boldsymbol{\theta}, t, \mathbf{y})$ as output

if in training stage or \mathbf{y} is ϕ **then**

$p_O(\cdot|\boldsymbol{\theta}; t) \leftarrow \text{softmax}(\Psi(\boldsymbol{\theta}, t, \mathbf{y}))_{dim=-1}$

else

 Input ($\boldsymbol{\theta}$, t , ϕ) to network, receive $\Psi(\boldsymbol{\theta}, t, \phi)$ as output

$p_O(\cdot|\boldsymbol{\theta}; t) \leftarrow \text{softmax}((1 + w)\Psi(\boldsymbol{\theta}, t, \mathbf{y}) - w\Psi(\boldsymbol{\theta}, t, \phi))_{dim=-1}$

end if

return $p_O(\cdot|\boldsymbol{\theta}; t)$

end function

Table 6: MAE on QM9 dataset w/ and w/o classifier-free guidance generation. Smaller errors are in **bold**.

	ϵ_{HOMO} / a.u.	ϵ_{LUMO} / a.u.	$\Delta\epsilon$ / a.u.
Conditional	0.00724	0.00981	0.01329
Unconditional	0.01901	0.04076	0.04104

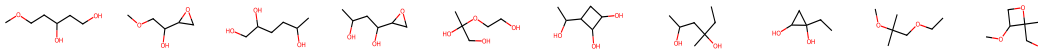


Figure 5: Conditioned samples on QM9. The number of sampling steps was 1k. Since QM9 exhaustively included stable small molecules made up of CHONF, only 4 conditioned samples and 5 unconditioned samples are novel.

3.3 Molecular Scaffold Extension

Here, we show a simple *inpaint* strategy can extend molecular scaffolds by using ChemBFN. In every sampling steps, parameters of input distributions are modified as $\boldsymbol{\theta} \leftarrow \mathbf{M} \odot \mathbf{e}_x + (1 - \mathbf{M}) \odot \boldsymbol{\theta}$ before being inputted into the network, where \mathbf{M} is the mask and \mathbf{e}_x is the one-hot representation of scaffold. Figure 6 shows an example of extending scaffold ‘Cc1cc(OC5)cc(C6)c1.’ by a model trained on MOSES SAFE³⁵ version, a variation of SMILES. We found that inpainting sampling for 10 to 100 steps was sufficient to generate complex molecules.

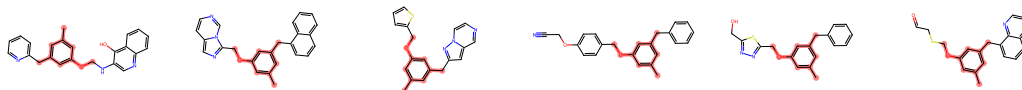


Figure 6: An example of extended molecular scaffold. The scaffold is highlighted in red.

3.4 Finetuning on Prediction Tasks

In this section, we compare our model with SOTA models,^{30,31,36-41} including graph-based and language-based which could be further classified as smaller scale natural language processing models (NLPs) and large language models (LLMs), on subsets of MoleculeNet benchmark. As shown in Table 7, our method outperformed SOTA language models on several tasks, especially ClinTox and BBBP. It is notable that ChemBERTa³⁰ and ChemBERTa-2,³¹ which had a similar model size with ours, were pretrained on 77M molecules but had worse scores on 3 out of 5 tasks than ours. This indicated that BFN-style generative pretraining is a better strategy than masked language modeling and multitask regression pretraining. A similar observation applied to CaR_{RoBERTa} model that coupled the knowledge of ChatGPT⁴² (which is far larger in scale than ours and is believed to have seen more chemical texts) and the distillation capability of RoBERTa²¹ method: our model outperformed CaR_{RoBERTa} on 4 out of 5 tasks. However, when comparing with graph neural networks (GNNs) our model performed averagely 1.7% worse, especially on regression tasks.

Table 7: Testing metrics on sub-tasks of MoleculeNet benchmark with **scaffold splitting** compared with SOTA models. The metrics of all other models were copied from their original paper. \uparrow indicates that the higher is better and \downarrow stands for the contrary. The best results are in **bold**. The best results within the same category (graph-based or language-based) are underlined. Percentages in the last two rows show the performance changes w.r.t the best models and the colour represents whether our model was better (in red) or not (in blue).

Method	ROC-AUC \uparrow				RMSE \downarrow			
	ClinTox	BBBP	BACE	HIV	ESOL	FreeSolv	Lipo	
GNNs	Uni-Mol ³⁶	<u>91.9</u>	72.9	85.7	80.8	0.788	<u>1.480</u>	0.603
	MolKD ³⁷	83.8	<u>74.8</u>	80.1	74.9	-	-	-
	GEM ³⁸	90.1	72.4	85.6	80.6	0.798	1.877	0.660
	Mole-BERT ³⁹	78.9	71.9	80.8	78.2	1.015	-	0.676
LLMs	CaR _{RoBERTa} ⁴⁰	84.16	81.99	<u>80.73</u>	-	0.96	-	1.02
	ChemBERTa ³⁰	73.3	64.3	-	62.2	-	-	-
NLPs	ChemBERTa-2 ³¹	60.1	74.2	79.9	-	-	-	<u>0.744</u>
	SMILES Transformer ⁴¹	-	70.4	70.1	72.9	-	-	-
	ChemBFN (ours)	99.18	95.74	73.56	<u>79.37</u>	<u>0.884</u>	1.418	0.746
	$\Delta_{GNN}^{s_{best}}$	+8%	+28%	-14%	-2%	+12%	-4%	+24%
	$\Delta_{LM}^{s_{best}}$	+18%	+17%	-9%	+9%	-8%	-	0%

3.5 Reaction Yield Prediction

In order to predict the reaction yield, we first trained the generative model to understand chemical reaction by learning to predict the products. We developed an *in-context* style guidance that during training stage only the parameters of product in reaction SMILES were predicted by always masking the input distribution of reactant/reagent and \gg token to the one-hot representation, i.e., $\theta \leftarrow M_{rr} \odot \mathbf{e}_x + (1 - M_{rr}) \odot \theta$, where M_{rr} is the mask for reactant, reagent, and \gg token.

The generative model was first pre-trained on USPTO-50k dataset then post-trained on Buchwald-Hartwig and Suzuki-Miyaura coupling datasets before the whole prediction model was fine-tuned. The testing scores compared with previous researches^{28,43,44} were reported in Table 8. It is notable that the Yield-BERT series^{28,44} were based on a pre-trained RXNFP⁴⁵ model which had been pre-trained on over 2M reactions while our model was pre-trained on 50k reactions. Despite the disadvantage of limited access of pretraining data, the performance of our method was still close to that of largely pretrained model on random-split sets and significantly better on out-of-sample predictions.

Table 8: R^2 scores on different testing sets of HTE Buchwald-Hartwig and Suzuki-Miyaura reaction datasets. The scores of all other models were copied from original paper. The best results are in **bold**. The score of “rand 70/30” split was the 10-fold average value. Test 1-4 were out-of-sample splits.

Dataset	Split	Method			
		MFF ⁴³	Yield-BERT ²⁸	Yield-BERT-DA ⁴⁴	ChemBFN (ours)
Buchwald-Hartwig	Rand 70/30	0.927 ± 0.007	0.951 ± 0.005	0.969 ± 0.004	0.952 ± 0.008
	Test 1	0.85	0.84	0.82	0.844
	Test 2	0.71	0.84	0.90	0.910
	Test 3	0.64	0.75	0.63	0.787
	Test 4	0.18	0.49	0.43	0.633
	Avg. 1-4	0.60	0.73	0.69	0.794
Suzuki-Miyaura	Rand 70/30	–	0.81 ± 0.02	–	0.796 ± 0.011

3.6 Is Larger Pretrain Dataset Better?

We have seen that our model, although was pretrained on 40M molecules, outperformed models pretrained on larger dataset on several prediction tasks. Here rises a question: whether larger pretrain dataset benefits our method? To answer this, 3 models were trained on AqSolDB dataset, of which one was trained from scratch, one was pretrained on 40M molecules from ZINC15 database, and one was pretrained on 190M molecules from ZINC15. We summarised the testing results in Table 9. Interestingly, the errors did not shrink when the pretrain data grew from 40M to 190M. However, compared with zero pretraining, an improvement on performance of $\geq 12.5\%$ can be confirmed.

Table 9: Testing metrics of models with different pretrain data sizes (0, 40M, and 190M) on AqSolDB dataset.

	From scratch	Pretrained on 40M	Pretrained on 190M
MAE	0.978	0.837	0.851
RMSE	1.309	1.131	1.145

3.7 Training Details

For all generative tasks, the models were trained for 100 epochs with the batch-size of 120 molecule/batch. The learning rate (lr) was 5.0×10^{-5} that was linearly increased (warm-up) from 10^{-8} during the first 1,000 training steps.

We pre-trained one model on 40M SMILES for 15 epochs with the batch-size of 512 on single A100 GPU and one model on 190M SMILES for 5 epochs with the effective batch-size of 1,024 (2×512) on $2 \times$ A100 GPUs. The warm-up strategy and lr were the same as mentioned above.

During fine-tuning stages, models were trained for 100 epochs on labelled datasets. The batch-size, both for training and validation, was 32 on MoleculeNet benchmark; the training batch-size was 16 for reaction yield prediction. lr_{max} was 10^{-4} that was warmed up from 10^{-7} during the first 1,000 steps for regression tasks and 100 steps for classification tasks. After warm-up stage, lr decreased by 0.2

after the validation metrics stopped improving for 20 epochs unless the learning rate had reached 10^{-6} . The dropout rate of prediction MLP head was fine-tuned for each case and we recommend to try from $\{0.0, 0.5, 0.7\}$. The validation metrics for regression and classification tasks were MAE and accuracy, respectively.

We employed AdamW⁴⁶ with default hyperparameters implemented in PyTorch⁴⁷ as the optimizer for all tasks.

4 Conclusion

ChemBFN, a Bayesian flow network framework for chemistry tasks of both generation and prediction, was developed in this work. The new accuracy schedule helped ChemBFN achieve competitive performance of discrete diffusion models and autoregressive models on generating large molecules. We proposed a BFN-style generative pretraining strategy that surpassed existing language-based transformer models on several classification and regression tasks. We believe this work provides a tool that can accelerate researches of both drug designing and filtering and give in helpful information for synthesis planning. However, we still leave gaps between graph-based models in prediction tasks, which we shall keep for the future research.

5 Acknowledgements

We show gratefulness to Research Center for Computational Science (RCCS), Okazaki, Japan and its maintenance team, who provided computing sources including A100 GPUs. This work is under project 24-IMS-C043 of RCCS. We also thank Dr. Maho Nakata who kindly lent us his own RTX 3080 GPU. Without the kindness of above mentioned people and team, this work would never be finished.

References

- [1] O. Prykhodko, S. V. Johansson, P.-C. Kotsias, J. Arús-Pous, E. J. Bjerrum, O. Engkvist and H. Chen, *Journal of Cheminformatics*, 2019, **11**, 74.
- [2] V. Bagal, R. Aggarwal, P. Vinod and U. D. Priyakumar, *Journal of Chemical Information and Modeling*, 2021, **62**, 2064–2076.
- [3] W. Jin, R. Barzilay and T. Jaakkola, International conference on machine learning, 2018, pp. 2323–2332.
- [4] N. Brown, M. Fiscato, M. H. Segler and A. C. Vaucher, *Journal of chemical information and modeling*, 2019, **59**, 1096–1108.
- [5] R. Mercado, T. Rastemo, E. Lindelöf, G. Klambauer, O. Engkvist, H. Chen and E. J. Bjerrum, *Machine Learning: Science and Technology*, 2020.
- [6] J. H. Jensen, *Chemical science*, 2019, **10**, 3567–3572.
- [7] H. Iwata, T. Nakai, T. Koyama, S. Matsumoto, R. Kojima and Y. Okuno, *Journal of Chemical Information and Modeling*, 2023, **63**, 7392–7400.
- [8] D. Polykovskiy, A. Zhebrak, B. Sanchez-Lengeling, S. Golovanov, O. Tatanov, S. Belyaev, R. Kurbanov, A. Artamonov, V. Aladinskiy, M. Veselov, A. Kadurin, S. Johansson, H. Chen, S. Nikolenko, A. Aspuru-Guzik and A. Zhavoronkov, *Frontiers in Pharmacology*, 2020.
- [9] J. Ho, A. Jain and P. Abbeel, *Advances in neural information processing systems*, 2020, **33**, 6840–6851.

- [10] C. Vignac, I. Krawczuk, A. Siraudin, B. Wang, V. Cevher and P. Frossard, *arXiv preprint arXiv:2209.14734*, 2022.
- [11] A. Graves, R. K. Srivastava, T. Atkinson and F. Gomez, *arXiv preprint arXiv:2308.07037*, 2023.
- [12] Y. Song, J. Gong, Y. Qu, H. Zhou, M. Zheng, J. Liu and W.-Y. Ma, *arXiv preprint arXiv:2403.15441*, 2024.
- [13] D. Weininger, *Journal of chemical information and computer sciences*, 1988, **28**, 31–36.
- [14] M. Krenn, F. Häse, A. Nigam, P. Friederich and A. Aspuru-Guzik, *Machine Learning: Science and Technology*, 2020, **1**, 045024.
- [15] A. Vaswani, N. Shazeer, N. Parmar, J. Uszkoreit, L. Jones, A. N. Gomez, L. u. Kaiser and I. Polosukhin, *Advances in Neural Information Processing Systems*, 2017.
- [16] W. Peebles and S. Xie, *Proceedings of the IEEE/CVF International Conference on Computer Vision*, 2023, pp. 4195–4205.
- [17] G. Klambauer, T. Unterthiner, A. Mayr and S. Hochreiter, *Advances in Neural Information Processing Systems*, 2017.
- [18] Y. Sun, L. Dong, B. Patra, S. Ma, S. Huang, A. Benhaim, V. Chaudhary, X. Song and F. Wei, *arXiv preprint arXiv:2212.10554*, 2022.
- [19] J. Su, M. Ahmed, Y. Lu, S. Pan, W. Bo and Y. Liu, *Neurocomputing*, 2024, **568**, 127063.
- [20] J. Devlin, M.-W. Chang, K. Lee and K. Toutanova, *arXiv preprint arXiv:1810.04805*, 2018.
- [21] Y. Liu, M. Ott, N. Goyal, J. Du, M. Joshi, D. Chen, O. Levy, M. Lewis, L. Zettlemoyer and V. Stoyanov, *arXiv preprint arXiv:1907.11692*, 2019.
- [22] S. Zhang, X. Zhang, H. Bao and F. Wei, *Attention Temperature Matters in Abstractive Summarization Distillation*, 2022.
- [23] R. Ramakrishnan, P. O. Dral, M. Rupp and O. A. Von Lilienfeld, *Scientific data*, 2014, **1**, 140022.
- [24] T. Sterling and J. J. Irwin, *Journal of chemical information and modeling*, 2015, **55**, 2324–2337.
- [25] Z. Wu, B. Ramsundar, E. N. Feinberg, J. Gomes, C. Geniesse, A. S. Pappu, K. Leswing and V. Pande, *Chemical science*, 2018, **9**, 513–530.
- [26] B. Ramsundar, P. Eastman, P. Walters, V. Pande, K. Leswing and Z. Wu, *Deep Learning for the Life Sciences*, O’Reilly Media, 2019.
- [27] N. Schneider, N. Stiefl and G. A. Landrum, *Journal of Chemical Information and Modeling*, 2016, **56**, 2336–2346.
- [28] P. Schwaller, A. C. Vaucher, T. Laino and J.-L. Reymond, *Machine Learning: Science and Technology*, 2021, **2**, 015016.
- [29] M. C. Sorkun, A. Khetan and S. Er, *Scientific data*, 2019, **6**, 143.
- [30] S. Chithrananda, G. Grand and B. Ramsundar, *arXiv preprint arXiv:2010.09885*, 2020.
- [31] W. Ahmad, E. Simon, S. Chithrananda, G. Grand and B. Ramsundar, *arXiv preprint arXiv:2209.01712*, 2022.
- [32] J. Ho and T. Salimans, *arXiv preprint arXiv:2207.12598*, 2022.
- [33] *RDKit: Open-source cheminformatics*, <https://www.rdkit.org>, Accessed: 2024-06-19.

- [34] Q. Sun, X. Zhang, S. Banerjee, P. Bao, M. Barbry, N. S. Blunt, N. A. Bogdanov, G. H. Booth, J. Chen, Z.-H. Cui *et al.*, *The Journal of chemical physics*, 2020, **153**, 024109.
- [35] E. Noutahi, C. Gabellini, M. Craig, J. S. C. Lim and P. Tossou, *Gotta be SAFE: A New Framework for Molecular Design*, 2023.
- [36] G. Zhou, Z. Gao, Q. Ding, H. Zheng, H. Xu, Z. Wei, L. Zhang and G. Ke, 2023.
- [37] L. Zeng, L. Li and J. Li, *arXiv preprint arXiv:2305.01912*, 2023.
- [38] X. Fang, L. Liu, J. Lei, D. He, S. Zhang, J. Zhou, F. Wang, H. Wu and H. Wang, *Nature Machine Intelligence*, 2022, **4**, 127–134.
- [39] J. Xia, C. Zhao, B. Hu, Z. Gao, C. Tan, Y. Liu, S. Li and S. Z. Li, The Eleventh International Conference on Learning Representations, 2022.
- [40] C. Qian, H. Tang, Z. Yang, H. Liang and Y. Liu, *arXiv preprint arXiv:2307.07443*, 2023.
- [41] S. Honda, S. Shi and H. R. Ueda, *arXiv preprint arXiv:1911.04738*, 2019.
- [42] J. Achiam, S. Adler, S. Agarwal, L. Ahmad, I. Akkaya, F. L. Aleman, D. Almeida, J. Altenschmidt, S. Altman, S. Anadkat *et al.*, *arXiv preprint arXiv:2303.08774*, 2023.
- [43] F. Sandfort, F. Strieth-Kalthoff, M. Kühnemund, C. Beecks and F. Glorius, *Chem*, 2020, **6**, 1379–1390.
- [44] P. Schwaller, A. C. Vaucher, T. Laino and J.-L. Reymond, 2020.
- [45] P. Schwaller, D. Probst, A. C. Vaucher, V. H. Nair, D. Kreutter, T. Laino and J.-L. Reymond, *Nature Machine Intelligence*, 2021, **3**, 144–152.
- [46] I. Loshchilov and F. Hutter, 2018.
- [47] A. Paszke, S. Gross, F. Massa, A. Lerer, J. Bradbury, G. Chanan, T. Killeen, Z. Lin, N. Gimeshein, L. Antiga, A. Desmaison, A. Kopf, E. Yang, Z. DeVito, M. Raison, A. Tejani, S. Chilamkurthy, B. Steiner, L. Fang, J. Bai and S. Chintala, *Advances in Neural Information Processing Systems*, 2019.